metals

MDPI

Article

Microstructural Control and Alloy Design for Improving the Resistance to Delayed Fracture of Ultrahigh-Strength Automotive Steel Sheets

Takehide Senuma [1,*], Mitsuhiro Okayasu [1] and Hardy Mohrbacher [2,3]

[1] Department of Mechanical and Systems Engineering, Okayama University, Okayama 700-8530, Japan; okayasu@okayama-u.ac.jp
[2] NiobelCon BV, B-2970 Schilde, Belgium; hm@niobelcon.net
[3] Department of Materials MTM, Leuven University (KU Leuven), 3001 Heverlee, Belgium
* Correspondence: senuma@mech.okayama-u.ac.jp

Abstract: The demand for higher-strength automotive steel sheets has increased significantly for lightweight and safe body concepts. However, the increment of the steel strength is often limited by the potential occurrence of delayed fracture. This paper discusses proper microstructure control and alloy design to improve the resistance against the delayed fracture of ultrahigh-strength automotive steel sheets in order to increase the usable upper limit of their strength and provides basic data serving as a practical guide for solving the problem of delayed fracture in ultrahigh-strength automotive steel sheets. It is confirmed that grain refinement, the appropriate dual-phase structure of martensite with ferrite or retained austenite, and surface decarburization, increase the resistance to delayed fracture. In terms of alloy design, the effects of Nb, Mo, and B on the delayed fracture resistance of hot-stamped steels have been investigated. The results suggest that there are other reasons for Nb to improve delayed fracture resistance in addition to grain refinement and the ability to trap hydrogen by its precipitates, as has been conventionally believed. Regarding Mo, it was clearly demonstrated that the segregation of this element at the grain boundary plays a main role in improving the delayed fracture resistance.

Keywords: delayed fracture; hydrogen embrittlement; high-strength steel; automotive steel sheets; microstructural control; alloy design

check for updates

Citation: Senuma, T.; Okayasu, M.; Mohrbacher, H. Microstructural Control and Alloy Design for Improving the Resistance to Delayed Fracture of Ultrahigh-Strength Automotive Steel Sheets. *Metals* **2023**, *13*, 1368. https://doi.org/10.3390/met13081368

Academic Editors: Chunfeng Hu and Giuseppe Lacidogna

Received: 25 June 2023
Revised: 23 July 2023
Accepted: 27 July 2023
Published: 29 July 2023

Copyright: © 2023 by the authors. Licensee MDPI, Basel, Switzerland. This article is an open access article distributed under the terms and conditions of the Creative Commons Attribution (CC BY) license (https://creativecommons.org/licenses/by/4.0/).

1. Introduction

For solving the conflicting interests of lighter car bodies and improved crashworthiness, automotive steels with higher strengths are required. A total of 1500 MPa class cold-rolled steel sheets [1] and 2000 MPa class hot-stamped steel sheets [2] have already been commercialized for the production of relevant components such as door impact beams, bumpers, and lateral impact parts.

Figure 1 shows an innovative car body design concept using next generation high-strength steel sheets recently released by Nippon Steel [3]. A significant reduction in sheet thickness, and thus body weight, can be achieved by using ultrahigh-strength steel sheets of 2000 MPa or higher. However, an important issue for the commercialization of these ultrahigh-strength steel sheets is the elimination of concerns regarding the occurrence of a delayed fracture. The delayed fracture is a phenomenon related to hydrogen embrittlement. The study of hydrogen embrittlement has a long history and many hypotheses on the mechanism of hydrogen embrittlement have been proposed.

In the case of the delayed fracture of ultrahigh-strength automotive steel components, the hydrogen ingress into the material is mainly due to corrosion, and the amount of diffusive hydrogen is in the sub-mass ppm range. In such a mild hydrogen embrittlement environment, the conceivable mechanisms of a delayed fracture are mainly the hydrogen-enhanced grain

boundary decohesion (HEGBDE) mechanism [4,5], the hydrogen-enhanced localized plasticity (HELP) mechanism [6–8], the absorption-induced decohesion (AIDE) mechanism [9], and the hydrogen-enhanced strain-induced vacancy (HESIV) mechanism [10]. As pointed out by Robertson et al. [11], the hydrogen embrittlement probably occurs, not by a single mechanism but rather by a combination of various mechanisms, with their different contribution ratios depending on the material, the amount of hydrogen, and the stress state.

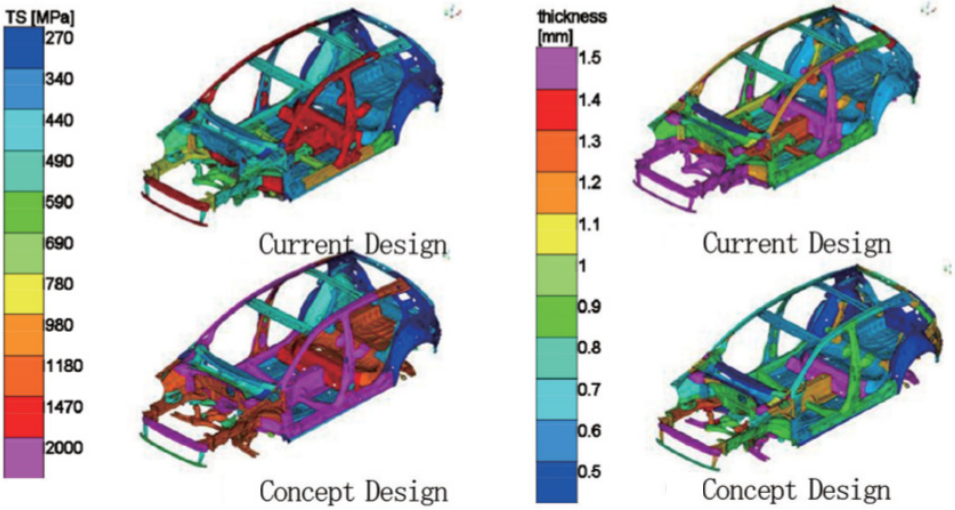


Figure 1. Comparison of material design between current and concept models [3].

In addition to the studies on the mechanism, metallurgical measures against a delayed fracture have been actively investigated to increase the resistance to the delayed fracture. From a microstructural point of view, it has been reported that a refinement of prior austenite grains reduces the susceptibility to the delayed fracture of martensitic steels [12–14]. These results were obtained on specimens of fresh martensitic steel or martensitic steel tempered at high temperatures. Since automotive steel parts inevitably undergo the bake hardening (BH) treatment (corresponding to a low-temperature tempering treatment), the formation of ferrous carbides and the amount of carbon segregated in the grain boundary are different from those of fresh martensitic steel or high-temperature-tempered martensitic steel. Therefore, the effect of grain refinement on the resistance to the delayed fracture of ultrahigh-strength automotive parts after BH treatment is investigated in this study.

Another microstructural measure against a delayed fracture is the application of a dual phase structure. Recently, martensitic steels with a high amount of retained austenite have been developed by a sophisticated heat treatment, the so-called Q&P (quench & partitioning) process to improve ductility [15]. This process has also been applied to the hot stamping process [16–18]. Since the susceptibility to the delayed fracture of cold- and hot-stamped Q&P steel parts has not been widely reported, we investigated it to elucidate the effect of this second phase on the resistance to the delayed fracture.

Another dual-phase variant of ultrahigh-strength steels represents a martensitic matrix with a small amount of ferrite. The amount of ferrite is controlled by the intercritical annealing temperature, i.e., the temperature between A_1 and A_3. In this study, the effect of a small amount of ferrite on the resistance to a delayed fracture is investigated.

Surface decarburization is another microstructural control of interest for ultra-high strength steel sheets, since it significantly improves their bendability. Bending is the main forming method for cold-rolled ultra-high strength steel sheets with a tensile strength of 1500 MPa and above [19]. Since the effect of decarburization on delayed fracture resistance has not been reported, this effect is also investigated in this study.

Many studies have been conducted to investigate the influence of alloy design on delayed fracture susceptibility. Microalloying elements are particularly effective in im-

proving the resistance against a delayed fracture. Respectively, this was reported for Nb [20–23], Mo [24–27], V [28–30], Ti [31–33] and combined additions of these elements, such as Nb-Mo [34–38], Nb-V [39–41], Nb-Ti [42], and Nb-Mo-Ti [43].

In most of the reported cases, alloy carbides were precipitated by tempering at high temperatures of around 600 °C. In these cases, most of the alloy carbides are not covered with cementite and act as an effective trap for hydrogen. Therefore, many researchers conclude that the improvement in delayed fracture resistance is due to grain refinement and hydrogen trapping caused by microalloy carbides. Similar conclusions have been reported for as-quenched hot-stamped materials with alloy carbides not covered by ferrous carbides. However, hot-stamped materials are tempered at relatively low temperatures during cooling or BH treatment. Hence, pre-existing microalloy carbides can be covered with nano-sized ferrous carbides. Therefore, the authors have investigated materials after BH treatment to determine the effects of microalloying elements on the delayed fracture properties of hot-stamped components. In this report, we report on the effects of Nb and Mo, which were particularly effective.

The purpose of this study is to elaborate a principal understanding by which engineers and researchers can counteract delayed fracture problems. In this respect, qualitative effects of microstructure control and alloy design are presented and discussed.

2. Materials and Methods

2.1. Materials

The chemical composition of the investigated steels is shown in Table 1. Steel A was industrially produced and provided by Nippon Steel Corporation. The other steels are produced in the laboratory using a vacuum furnace. The procedure of preparing the specimens for the microstructure control experiment is described in Section 3. The samples investigating the influence of alloying elements were produced as follows: 50 Kg ingots were reheated to 1250 °C (with exception Steel Nb4 which was reheated to 1300 °C) and held for 60 min to dissolve the Nb precipitates and hot-rolled to 2.8 mm thick hot bands at a finishing temperature of around 930 °C. The hot band was placed directly in an electric furnace and held at 400 °C in the case of Mo-containing steels or 600 °C for other steels for 60 min and cooled to room temperature with the furnace switched off. After pickling, the hot bands were cold rolled to a thickness of 1.4 mm. The cold-rolled steel sheet was subjected to a heat treatment replicating the conditions of a hot stamping process. The heat treatment was conducted using a direct current heater. The samples were heated at 10 °C/s to various temperatures and held at various time periods. Subsequently, they were quenched using by water spraying. The samples were then BH-treated at 170 °C for 20 min.

Table 1. Chemical composition of the steels used in the experiments (mass %).

Steel	C	Si	Mn	Nb	Mo	Cr	Ti	B	N
A	0.22	0.1	1.2	0	0	0.15	0.01	0.002	
B	0.31	0.98	2.5	0.02	0	0	0.01	0.002	0.0010
C	0.35	0.1	1.2	0	0	0	0.01	0.002	0.0006
Nb1	0.32	0.1	2.5	0	0	0	0.01	0.002	0.0005
Nb2	0.32	0.1	2.5	0.025	0	0	0.01	0.002	0.0005
Nb3	0.32	0.1	2.5	0.05	0	0	0.01	0.002	0.0006
Nb4	0.32	0.1	2.5	0.075	0	0	0.01	0.002	0.0007
Mo1	0.32	0.1	1.2	0	0	0	0.01	0.002	0.0020
Mo2	0.33	0.1	1.2	0	0.15	0	0.01	0.002	0.0022
Mo3	0.33	0.1	1.2	0	0.3	0	0.01	0.002	0.0021
Mo4	0.33	0.1	1.2	0	0.5	0	0.01	0.002	0.002
B0	0.32	0.1	2.5	0.05	0	0	0.01	0	0.001
NM	0.32	0.1	1.2	0.05	0.5	0	0.01	0.002	0.001

All steels are Al-killed by adding 0.035–0.042% Al. P: 0.001–0.005%, S: 0.001–0.005%.

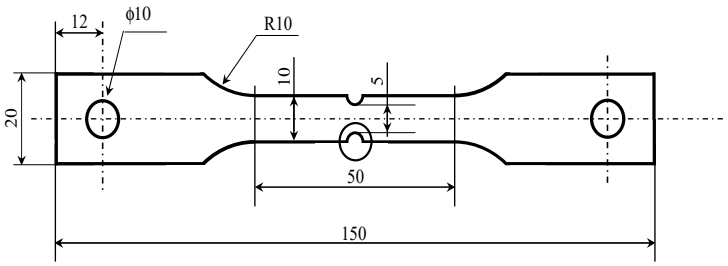
2.2. Mechanical Testing

The samples used for mechanical testing were ground from 1.4 to 1.0 mm thickness to avoid the effect of possible unintended decarburization during heat treatment. The tensile test was performed using samples in accordance with the Japanese standard JIS 13B and a universal tensile testing machine, AG-50kNXplus, Shimazu Ltd. At least two tests were performed for each steel, and the plotted value is the mean value.

The delayed fracture test was carried out by immersing samples in 10% or 20% ammonium thiocyanate solution under a maximum stress of approximately 0.65 × TS at the notch of the sample. The time to fracture was measured as a performance criterion. Figure 2 shows the facility and the sample used for the delayed fracture test. The sample was placed in the camber shown in the center of the equipment containing the ammonium thiocyanate solution. Dead weights are placed on the back of the facility to apply a constant stress to the sample. Since the scattering in experimental results was relatively high, the number of tests per steel was increased up to seven. Reported values represent the average of these individual tests.



(**a**)



(**b**)

Figure 2. Testing facility (**a**) and size of the specimen of the delayed fracture test (**b**).

2.3. Microstructural Observations and Analysis

The microstructure was characterized using optical microscopy (OM) and secondary electron microscopy (SEM), JSM-700IF, JEOL. Transmission electron microscopy (TEM) was used to determine the size and distribution of precipitates. TEM foils were prepared by the

standard twin-jet electropolishing method with an applied voltage of 20 V using a 300 mL of methanol, 180 mL of n-butanol, and 30 mL of perchloric acid electrolyte at –40 °C. Bright field (BF), dark field (DF), and selected area diffraction (SAD) images were obtained using a Topcon EM-002B operating at 160 kV.

Microtexture data obtained by electron backscatter diffraction pattern (EBSP) analysis were used to determine details of martensite structure such as prior austenite grain size, packet, and block size. The prior austenite grain size was determined by analyzing the EBSP measurement data using the software developed by Miyamoto et al. [44].

A three-dimensional atom probe (3DAP) was used to investigate the grain boundary segregation behavior. The 3DAP measurements were performed using the laser mode of a local electrode atom probe with a high-angle reflection (LEAP X4000X HR), where the frequency was 250 kHz and the pulse energy was 30 pJ. The specimen temperature was set to 50 K.

2.4. Measurement of Hydrogen Accumulated in the Sample

To measure the total amount of accumulated hydrogen, the sample was immersed in 10% or 20% ammonium thiocyanate solution for 48 h. The accumulated hydrogen was determined by thermal desorption analysis (TDA) by means of a gas chromatograph (JTF-20AH), J-Scence. The heating rate was 200 °C/h. The number of measurements ranged from two to five for each of the investigated steels.

3. Results and Discussion

3.1. Effect of Microstructures on the Resistance to Delayed Fracture

3.1.1. Effect of Grain Refinement

Samples were prepared from an Al-Si-coated cold-rolled steel sheet of Steel A. The samples were heated to 900 °C, 1000 °C, and 1200 °C at a rate of 10 °C/s to vary the grain size. Immediately after reaching the heating temperatures, the samples were quenched and then BH treated. The delayed fracture tests were carried out in 20% ammonium thiocyanate solution under an applied stress of 1 GPa at the notch of the sample, and the time to the fracture was measured. Figures 3 and 4 show the results of the tensile and delayed fracture tests, respectively. Both the tensile strength and the time to the delayed fracture increased, and decreased prior to the austenite grain size. Hence, grain refinement is not only beneficial for strengthening the steel (Hall–Petch effect) but simultaneously reduces the susceptibility to the delayed fracture. This result confirmed that the grain refinement of BH-treated samples such as hot-stamped ultrahigh-strength automotive parts also improves the resistance to a delayed fracture, even though the state of ferrous carbides and the amount of carbon segregated in the grain boundary are different from that of fresh martensitic steel or martensitic steel tempered at high temperatures.

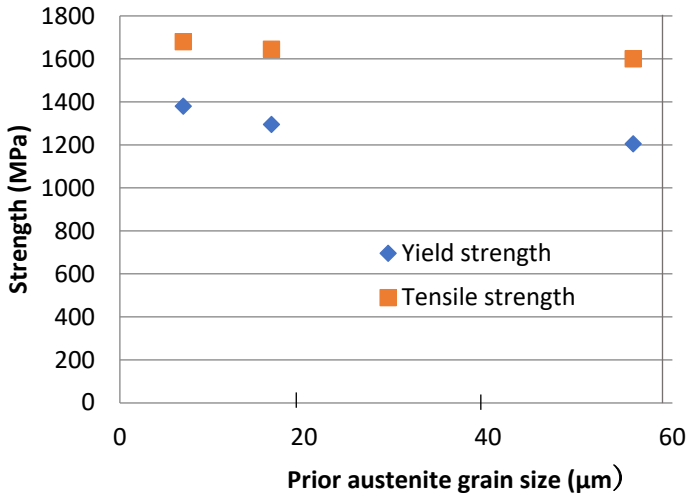


Figure 3. Effect of prior austenite grain size on yield strength and tensile strength.

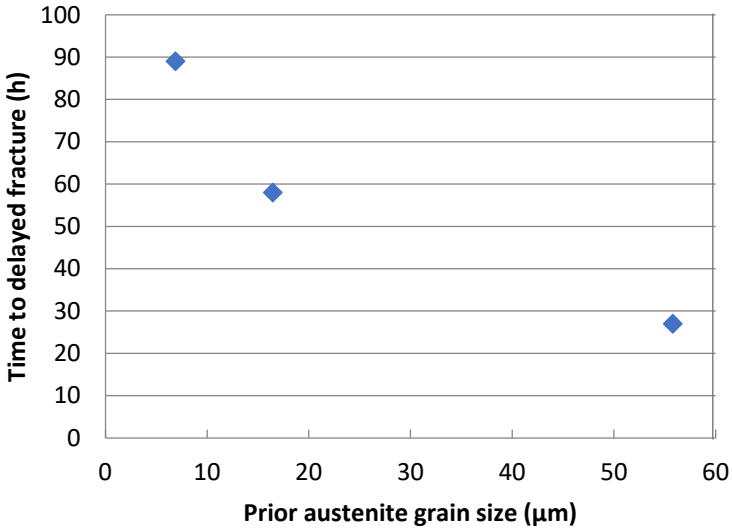


Figure 4. Effect of prior austenite grain size on the time to delayed fracture.

Detailed observations of the microstructure and measurements of hydrogen accumulated in the steel after immersion in 20% ammonium thiocyanate solution for 48 h were performed to interpret the experimental results.

The prior austenite grain size and the results of hydrogen measurements of the samples heated to the various temperatures are given in Table 2. The calculated amount of hydrogen per unit grain boundary area is also presented. The total amount of hydrogen stored in the samples increases with the prior decreasing austenite grain size. However, the amount of hydrogen stored per unit grain boundary area decreases with decreasing the prior austenite grain size. Similar to hydrogen, the amount of embrittling elements such as the P and S per unit grain boundary area is also reduced by grain refinement. These facts indicate that grain refinement suppresses the risk of grain boundary decohesion and thus improves the delayed fracture resistance, suggesting that the HEGBDE mechanism plays an important role.

Table 2. Amount of hydrogen stored in samples with different prior austenite grain size.

Prior Austenite Grain Size (μm)	6.88	16.45	55.75
Accumulated Total Hydrogen Content (mass ppm)	7.00	5.82	5.50
Hydrogen Content per Unit Grain Boundary Area (mass ppm/m^2)	48.7	83.6	387

Figure 5 shows the configuration of high angle boundaries (misorientation of 15° or higher) reconstructed by a software analysis of EBSP for the samples with an average prior austenite grain size of 6.88 μm and 55.78 μm, respectively. High angle boundaries act as a barrier to crack propagation and suppress the plastic deformation that creates excess vacancies. This implies that the contribution of the HESIV mechanism to the delayed fracture is reduced by grain refinement.

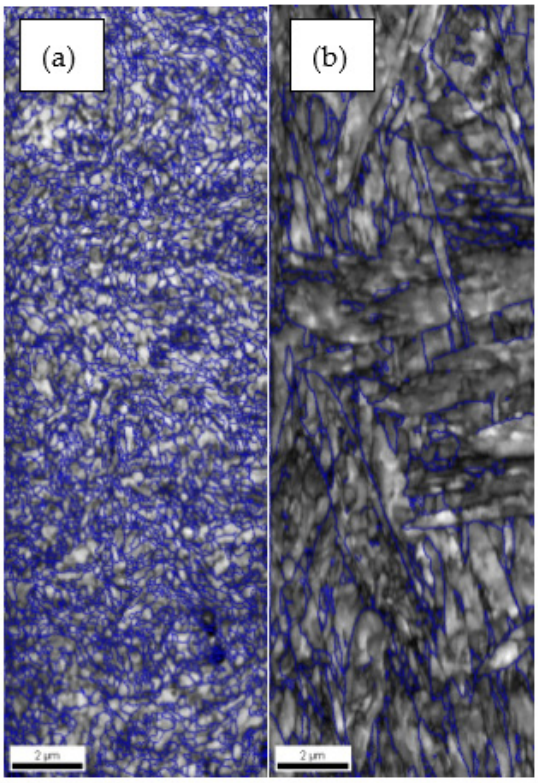


Figure 5. IQ maps showing high angle boundaries more than 15° (blue lines) in the samples heated to 900 °C (**a**) and 1200 °C (**b**).

3.1.2. Dual Phase Structure

Effect of Retained Austenite

For this experiment, Steel B containing 0.98% Si is used. The cold-rolled sample was heat-treated as shown in Figure 6, representing a typical Q&P process. The sample achieved a tensile strength of 1490 MPa, a uniform elongation of 21.5%, and a total elongation of 23% after the BH treatment. Assuming that a cold-stamped steel component experiences a maximum thickness reduction of 15%, a sample for the delayed fracture test was prepared from a tensile test sample strained by 15%. In addition, an unstrained sample after Q&P treatment and a sample heated to 900 °C at a rate of 10 °C/s and quenched were also prepared. The latter sample has a tensile strength of 2032 MPa after BH treatment.

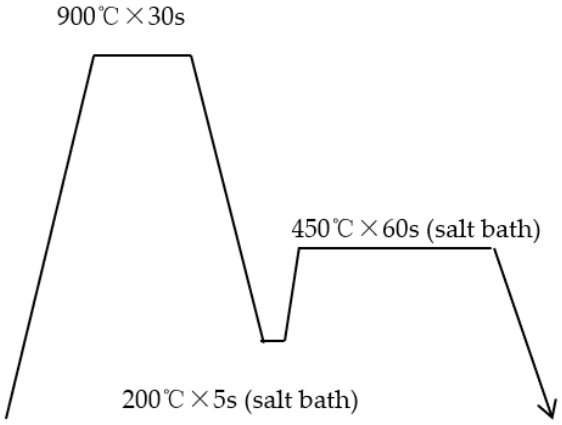


Figure 6. Thermal history of the quenching and partitioning treatment conducted in the experiment.

A delayed fracture test was performed by immersing the sample in a 10% ammonium thiocyanate solution, then stressing to 0.65 × TS at the notch machined in the center of the sample and measuring the time to fracture. As shown in Figure 7, the Q&P sample without straining has an excellent resistance to the delayed fracture (the test was interrupted after a duration of 400 h without failure). The 15% strained Q&P sample, however, has a much higher susceptibility to the delayed fracture, which is rather comparable to the as-quenched steel with 2000 MPa strength. These observations indicate that, depending on the severity of the press-forming, a cold-stamped automotive component manufactured from a retained austenite containing a ultrahigh-strength steel sheet with high ductility such as a Q&P steel sheet is inferior to one made of a hot-stamped steel sheet, not only in terms of shape fixability but also in terms of its susceptibility to a delayed fracture.

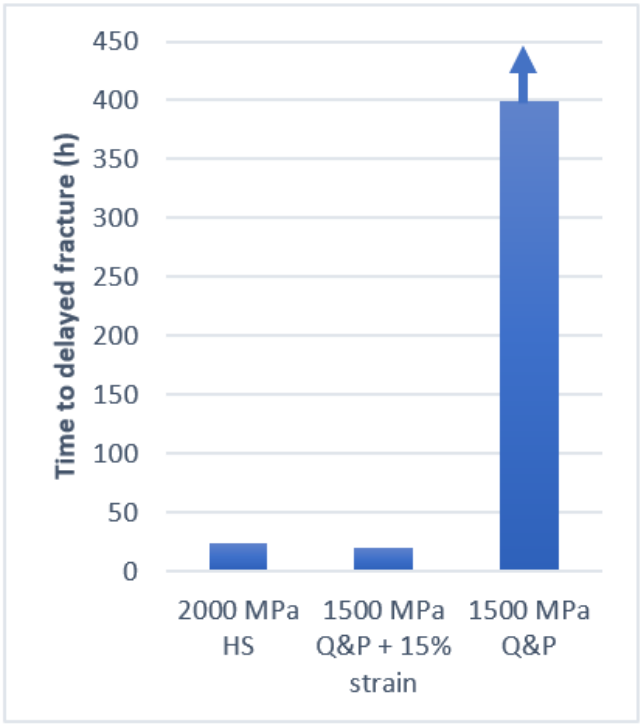


Figure 7. Time to delayed fracture of samples of 2000 MPa class hot-stamped steel sheet, and 1500 MPa class Q&P steel sheets before and after 15% straining.

The limited delayed fracture resistance of the steel in a 15% strained condition must be related to the formation of strain-induced martensite. The retained austenite share derived from EBSP data was reduced from 14% to 6%, thus the difference must have transformed into martensite. The transformation of retained austenite into martensite creates large local tensile stress fields in the steel matrix, and is detrimental in conjunction with diffusible hydrogen. The excellent delayed fracture resistance of the unstrained Q&P sample is due to the high hydrogen trapping ability of austenite and the absence of transformation-induced stress fields.

The results presented indicate that hot stamping combined with a subsequent Q&P process after forming is a promising method for producing ultrahigh-strength automotive parts with high resistance to a delayed fracture.

Effect of Ferrite

When quenching an austenitized steel from just below the A_3 temperature, the resulting martensitic microstructure contained a small amount of ferrite. The presence of such a small amount of ferrite has been reported to enhance the susceptibility to a delayed fracture [45], while the opposite effect has also been noted [46,47]. A detailed review of

these reports suggested to investigate the effect of ferrite on the susceptibility to a delayed fracture, thereby considering the morphology of the ferrite islands in the martensitic matrix. The samples for this investigation were obtained from cold-rolled and hot-dipped steel sheets of Steel A, respectively. The cold-rolled steel sheet had a deformed microstructure whereas the hot-dipped aluminized steel sheet revealed a recrystallized microstructure. Both samples were heated to 790 °C and held for 60 s before quenching. The cold-rolled sample was designated as 790 °C-CR and the recrystallized sample was designated as 790 °C-AS, respectively. A reference sample was prepared by heating the cold-rolled steel sheet to 900 °C at a rate of 10 °C/s and quenching it, and this sample was designated as 900 °C-CR.

Figure 8 shows the microstructures of all three samples. While Sample 900 °C-CR has a fully martensitic microstructure, the other samples show a dual phase microstructure with a small amount of ferrite (~10%). The morphology of the ferrite in Sample 790 °C-CR appears as relatively coarse, pancaked ferrite grains aligned with the rolling direction. On the contrary, the ferrite phase in Sample 790 °C-AS was finely dispersed. Although the strength of the ferrite is low, the strength of the ferrite containing samples was nearly equal to the fully martensitic steel. When quenching from below the A_3 temperature, the formation of ferrite results in carbon partitioning so that the carbon concentration in the remaining austenite is increased. Accordingly, the strength of this carbon-enriched martensite is increased after quenching, mitigating the softening effect of the coexisting small amount of ferrite.

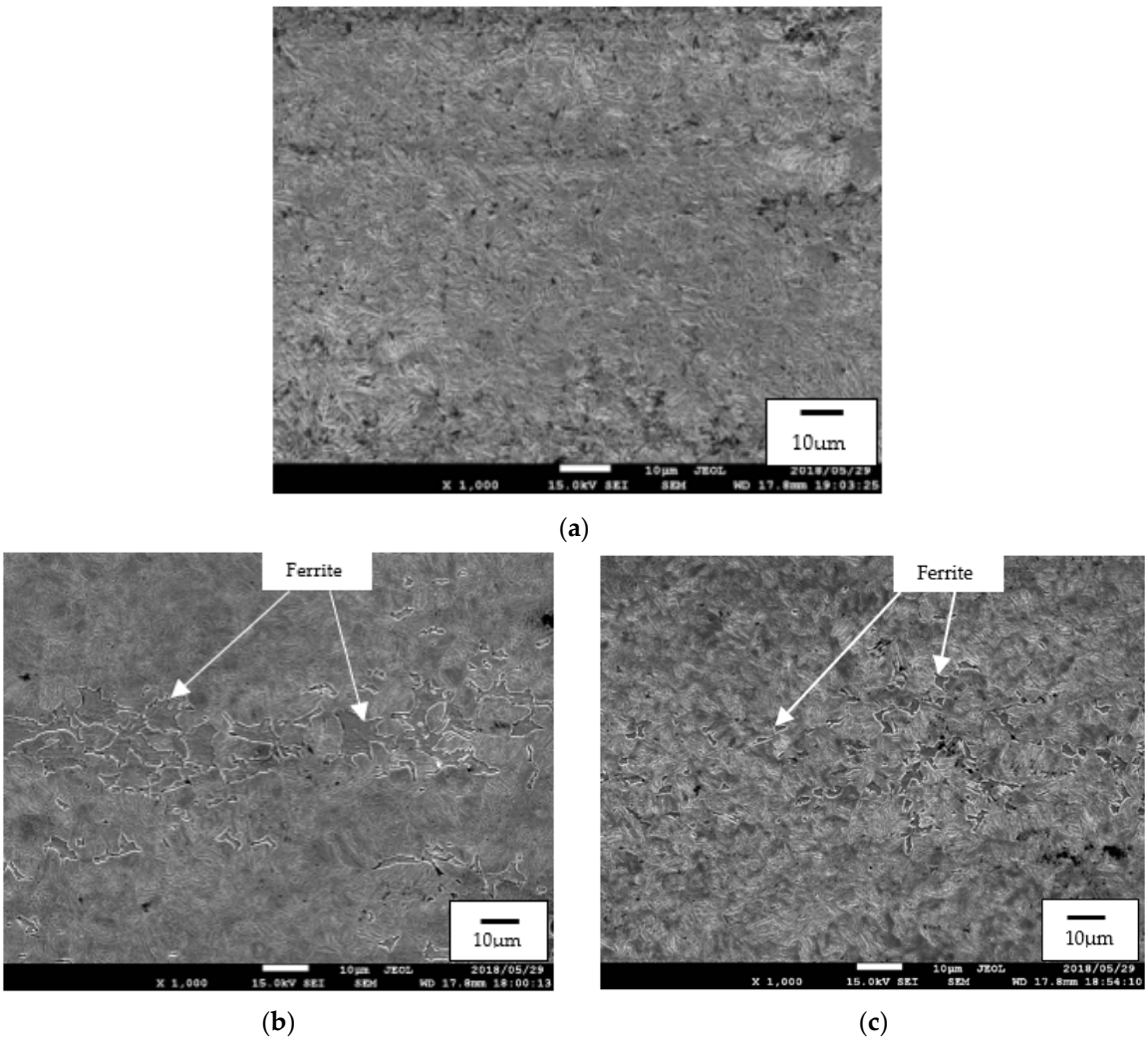


Figure 8. Microstructures of Samples: 900 °C-CR (**a**), 790 °C-CR (**b**), and 790 °C-AS (**c**).

Delayed fracture tests were performed by immersing the test sample in a 10% ammonium thiocyanate solution, then applying a stress of 1 GPa to the notch machined in the center of the sample and measuring the time to fracture.

Figure 9 shows the results of the delayed fracture tests of the samples after BH treatment. It appears that the delayed fracture time of sample 790 °C-CR with relatively large-sized elongated ferrite grains is shorter than that of the reference sample as well as that of sample 790 °C-AS with finely dispersed ferrite which did not break within a 200 h. Thus, it is evident that the morphology of ferrite must have a strong effect on the delayed fracture resistance. The amount of hydrogen absorption measured in a sample immersed in 20% ammonium thiocyanate for 48 h was not significantly influenced by the presence of ferrite (around 0.6 mass ppm ±10%). Hence, the improvement in delayed fracture resistance due to the presence of finely dispersed ferrite grains is presumably due to the local stress concentration being efficiently relaxed by the ferrite. In contrast, when the relatively large ferrite grains with inhomogeneous distribution as appearing in Sample 790 °C-CR, the relaxation of the local stress concentration is insufficient. Furthermore, the continuous aligned ferrite/martensite interface facilitates crack propagation, potentially accelerating the delayed fracture.

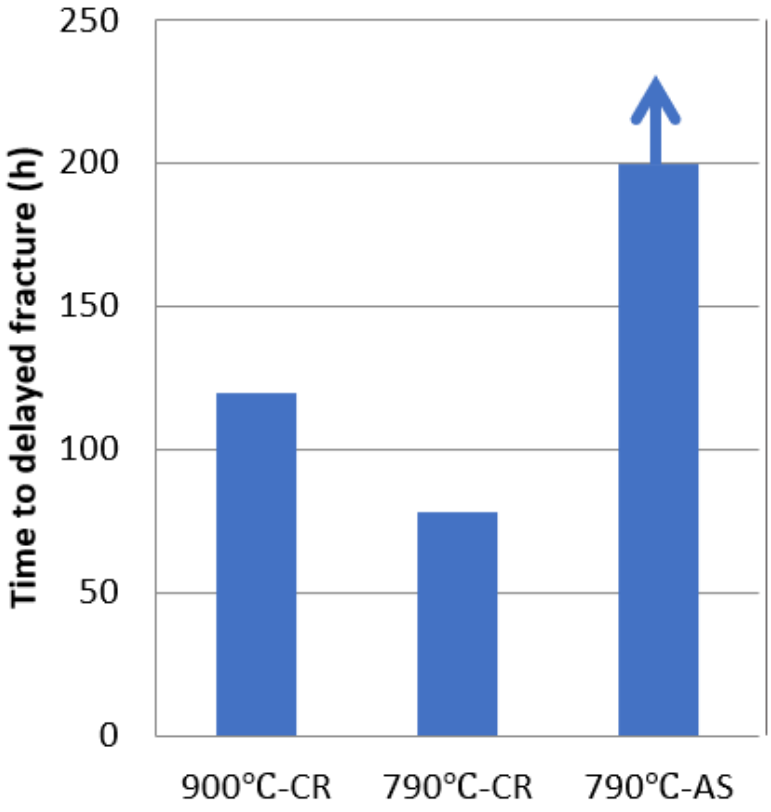


Figure 9. Effect of ferrite in the martensitic matrix and its morphology on the time to delayed fracture (Sample 790 °C-AS, in which ferrite was finely dispersed, did not break within 200 h).

3.1.3. Effect of Surface Decarburization

Steel C was used to study the effect of decarburization on the resistance to the delayed fracture. A decarburized surface layer must be formed at the notch of the sample, which is the starting point of the fracture. Therefore, the sample was first machined to the profile shown in Figure 2 and then decarburized. For decarburization, samples were heated at 790 °C for 20 min in a 100% hydrogen atmosphere with a dew point of 57 °C, whereas the reference samples were heated at 790 °C for 20 min in a 100% nitrogen atmosphere with a dew point of −38 °C. Both samples demonstrated a metallic surface, and significant scale

formation was not observed. The samples were lightly pickled with hydrochloric acid and then BH-treated.

The microstructure of the decarburized sample is shown in Figure 10. The reference sample had no decarburized layer and revealed a full martensitic microstructure, whereas the decarburized sample had the 55 μm thick decarburized zone.

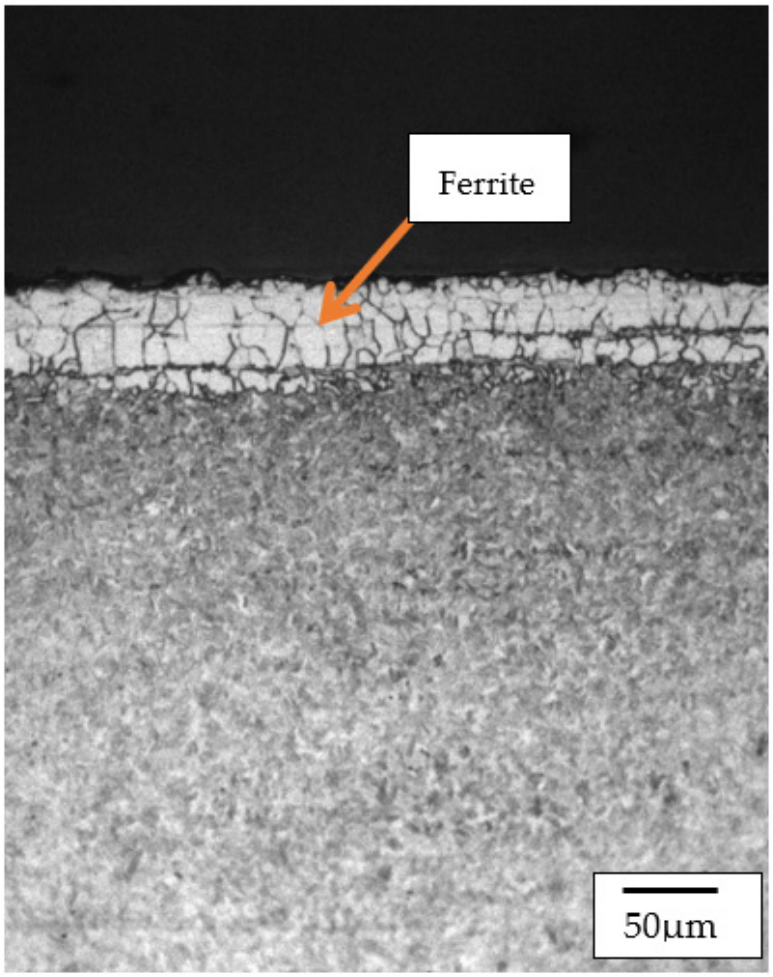


Figure 10. Microstructure in the vicinity of surface of the decarburized sample of Steel C heated at 790 °C for 20 min and quenched (the matrix is martensite).

Figure 11 shows the results of the delayed fracture tests by immersing the specimen in a 10% ammonium thiocyanate solution under a maximum stress of 1300 MPa at the bottom of the notch of the specimen.

These results clearly indicate that surface decarburization strongly enhances the resistance to a delayed fracture. A possible explanation for this improvement might be related to the decarburized layer suppressing the penetration of hydrogen from the surface towards the bulk. To examine this hypothesis, the amount of hydrogen was measured in the decarburized sample and non-decarburized sample which were BH-treated and then immersed in a 10%-NH4CN solution for 1 and 3 h. However, as evidenced by Figure 12, the presence of the decarburized layer facilitates the penetration of hydrogen into the sample. Another conceivable reason is that the softer surface layer of ferrite suppresses the propagation of the crack initiated at the interface between the ferrite and martensite phases. This phenomenon was observed in the bending test samples subjected to the same decarburization treatment, as shown in Figure 13.

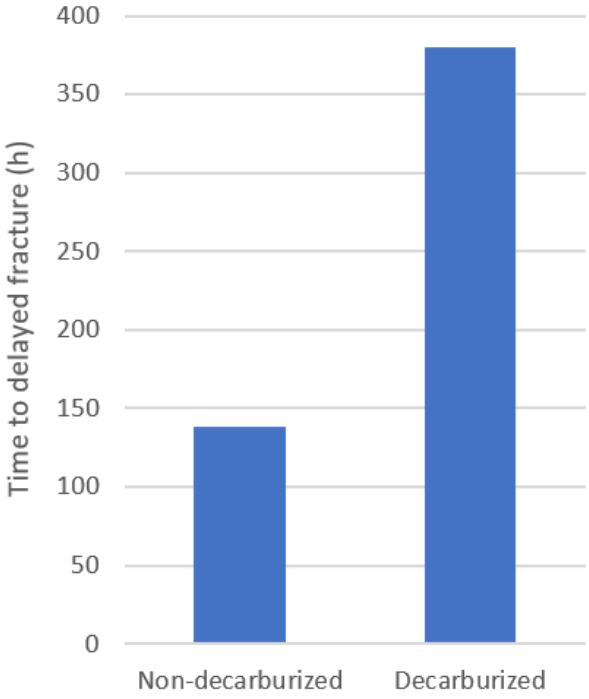


Figure 11. Effect of decarburization on time to delayed fracture of reference and decarburized samples of Steel C heated at 790 °C for 20 min and quenched and subjected to BH treatment.

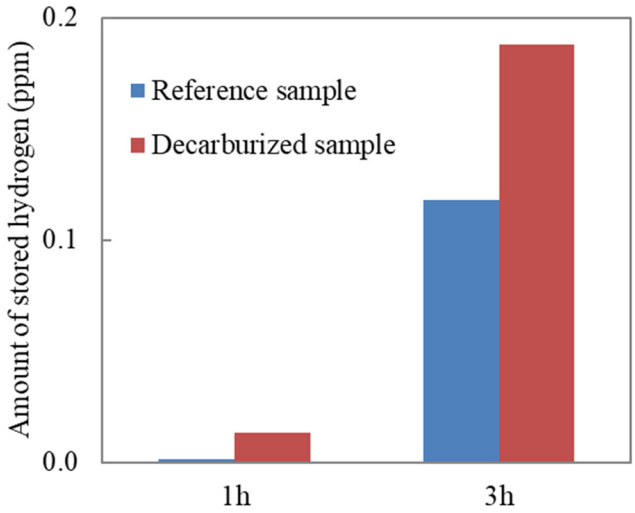


Figure 12. Amount of hydrogen stored in the decarburized and non-decarburized samples of Steel C, which were BH-treated and then immersed in a 10%-NH4CN solution for 1 and 3 h.

3.2. Effect of Microalloys on the Resistance to Delayed Fracture

The addition of microalloying elements is effective in improving delayed fracture resistance. Microalloying elements enhance the delayed fracture resistance in both constitutions, namely in a solid solution and as carbide precipitates. In the solute condition, they affect grain boundary cohesion, dislocation mobility, hydrogen diffusion, grain refinement and vacancy diffusion. Nano-sized carbide precipitates have an influence on hydrogen trapping ability, dislocation mobility, and grain refinement.

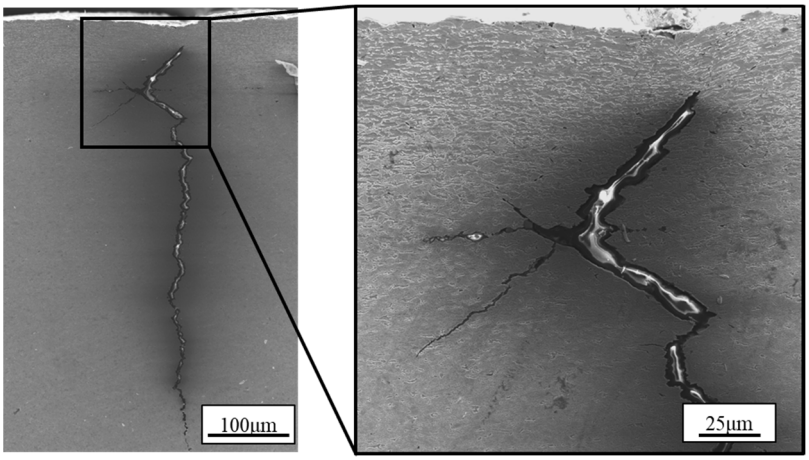


Figure 13. State of a crack observed in a bending test sample (the left figure is an overall view of the crack, and the right figure is an enlarged view of the crack initiation position).

Although many publications report the beneficial effects of microalloying elements on delayed fracture resistance, few articles separately analyze the contribution of each of the above effects. These particular effects on the resistance to the delayed fracture were investigated and analyzed for Nb and Mo as representative microalloying elements using steels Nb1-4 and Mo1-4.

Figure 14 shows the effect of the prior austenite grain size on the time to the delayed fracture of hot-stamped Nb-containing ultrahigh-strength steels along with data for the Nb-free steel with various grain sizes. The test samples were immersed in a 10% ammonium thiocyanate solution during the delayed fracture test. The samples of the Nb-containing steels were heated at 10 °C/s to 825 °C and immediately quenched with water. The grain size of the Nb-free steel was varied by adjusting the heating temperatures to 825 °C, 1000 °C, and 1100 °C, respectively. The tensile strength of the specimens after BH treatment was about 2000 MPa in all cases. From Figure 14, it appears that the increase in the resistance to a delayed fracture of steels containing Nb cannot be solely explained by the grain refinement effect. The deviation of the Nb-microalloyed steels from the pure grain size relationship must be caused by additional interactions of Nb.

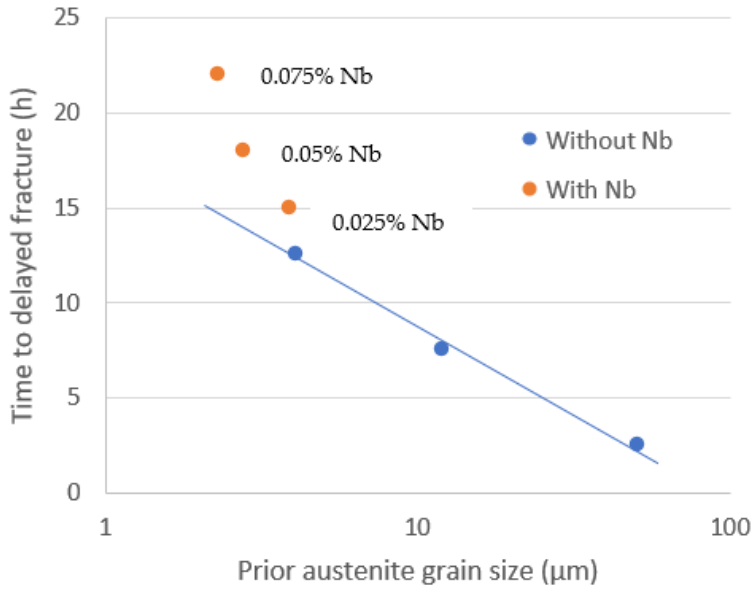


Figure 14. Influence of prior austenite grain size on time to delayed fracture of the steels with and without Nb addition.

One of these effects is thought to be the ability of NbC nano-sized precipitates to trap hydrogen. Therefore, the stored hydrogen content was measured by immersing the specimens in a 10% ammonium thiocyanate solution for 48 h after BH treatment. However, the Nb content had little effect on the amount of stored hydrogen, as shown in Figure 15, although the amount of NbC increased with the increasing Nb content, meaning that the assumed hydrogen trapping ability of the microalloy carbides was not exploited. This finding is inconsistent with the results obtained by using hot-stamped ultra-high strength steels without BH treatment [20,21,27] and those obtained by using ultra-high strength steels tempered at high temperatures [42]. To elucidate this inconsistency with the reported results, the precipitation state of NbC was investigated by TEM.

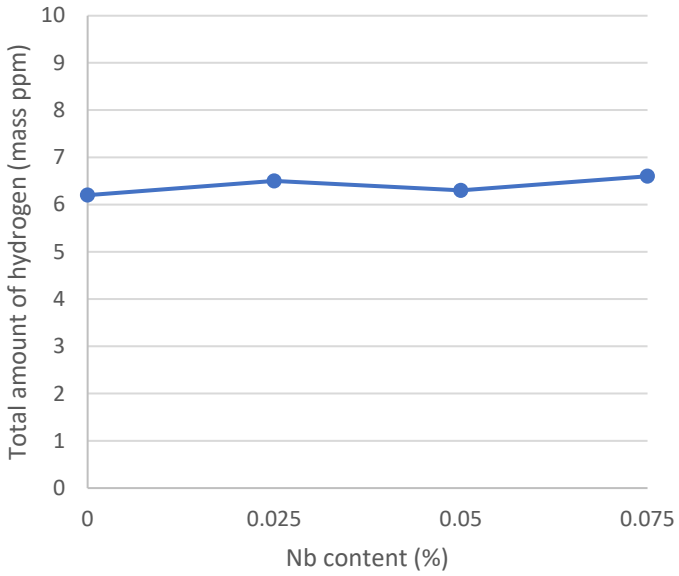


Figure 15. Influence of the Nb content on the total amount of stored hydrogen in samples immersed in a 10% ammonium thiocyanate solution for 48 h after BH treatment.

Figure 16 shows ferrous ε-carbide and NbC precipitates in the Nb3 steel after BH treatment, respectively. Using the different orientation relationships with the matrix, the ε-carbide and NbC could be displayed separately in the DF images. It was recognized that most of the NbC precipitates are covered with nanosized ε-carbide. The amount of ferrous carbide precipitated during the BH treatment depends on the carbon content, which was the same among the steels used in the experiment. Assuming that the interface between the ferrous carbide and the matrix is the trapping site of hydrogen, it is understandable that a significant difference in the amount of stored hydrogen was not observed among the steels. This result implies that the hydrogen trapping ability of NbC is largely suppressed by the coverage with ε-carbide and hardly contributed to the increase in the resistance to the delayed fracture of hot-stamped and subsequently BH-treated ultrahigh-strength Nb steels, contrary to the as-quenched condition.

The other possible mechanism for improving the resistance to a delayed fracture is related to the improvement of the grain boundary cohesion by solute Nb. Although a 3DAP measurement demonstrated that Nb hardly segregated at the grain boundary, the Nb content in the grain boundary is equal to the amount added or little higher. On the other hand, a thermodynamic calculation of the grain boundary segregation of alloying elements indicates that the amount of C and B segregated on the grain boundary increases by adding Nb [48]. Both C and B are known to enhance grain boundary cohesion. The Nb addition may indirectly increase the grain boundary cohesion and thus improve the resistance to the delayed fracture.

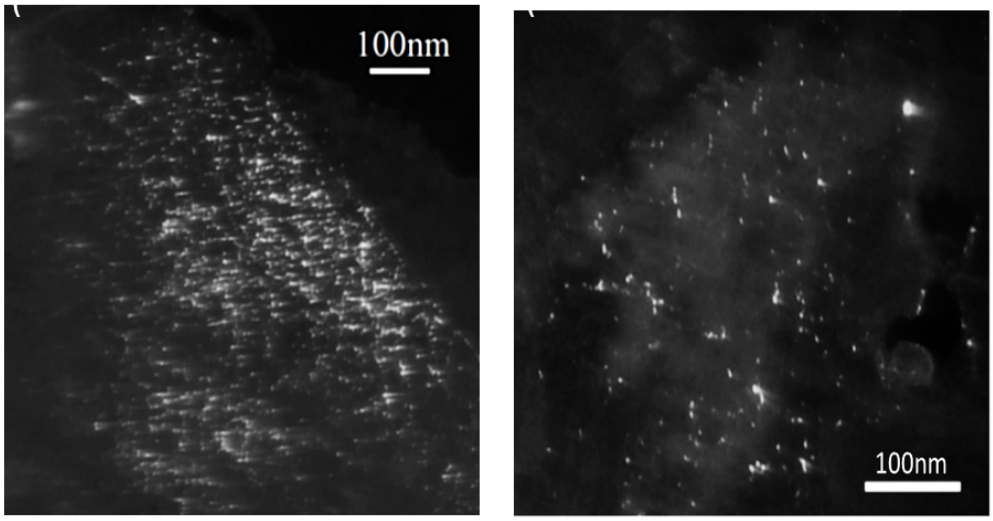


Figure 16. Precipitates in Steel Nb 3 containing 0.5% Nb after BH treatment observed by thin foil transmission dark-field electron microscopy.

Figure 17 shows the effect of the prior austenite grain size on the time to the delayed fracture of hot-stamped Mo containing ultrahigh-strength steels (Steels Mo2-Mo4) together with the data of the Mo-free steel with different grain size (Steel Mo1). The samples were heated at 10 °C/s to 875 °C and quenched immediately after heating. The test samples were immersed in a 10% ammonium thiocyanate solution during the delayed fracture test. The samples of the Mo-containing steels were heated to 10 °C/s to 875 °C and immediately quenched with water. The grain size of the Mo-free steel was varied by adjusting the heating temperature. As in the case of Nb, the increase in resistance to the delayed fracture of Mo-containing steels cannot be explained solely by the grain refinement effect. The deviation of the Mo-containing samples from the pure grain size relationship was even larger than that of the Nb-containing steels.

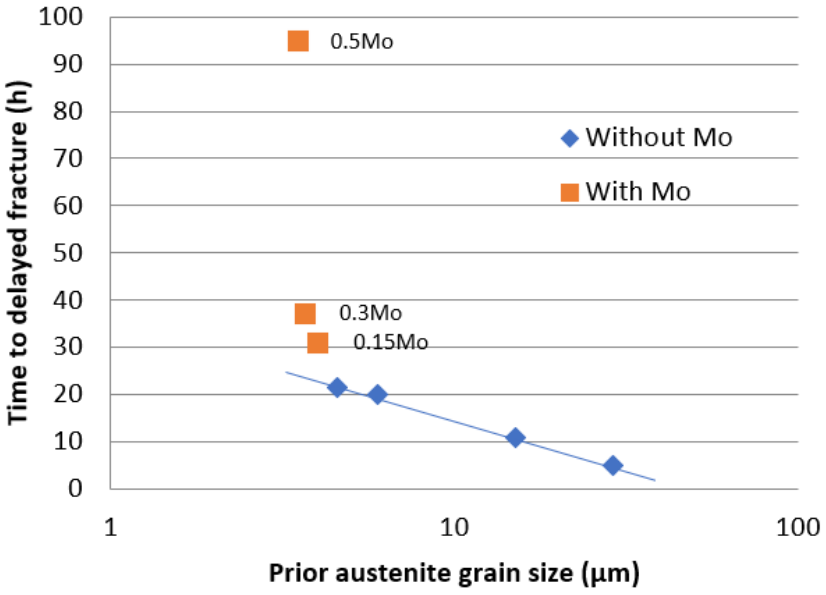


Figure 17. Effect of prior austenite grain size on time to delayed fracture of samples with and without Mo heated to 875 °C at 10 °C/s, quenched, and then BH treated.

Figure 18 shows the total amount of hydrogen stored in the samples immersed in a 10% ammonium thiocyanate solution for 48 h after BH treatment. Accordingly, the increase in the Mo content has a little effect on the accumulated amount of hydrogen. The Mo steels in this case do not contain Mo carbides because the coiling temperature of the hot band was 400 °C. Mo carbides cannot precipitate at that temperature, and in addition, the cold-rolled samples were heated to a temperature above the solution temperature of Mo carbides. It has been reported [26,37] that Mo, in a solution, traps hydrogen and retards the diffusion of hydrogen, thereby increasing the resistance to a delayed fracture. However, this result indicates that the hydrogen-trapping ability of Mo in a solution is not high, and the solute Mo does not play a significant role in improving the resistance to a delayed fracture.

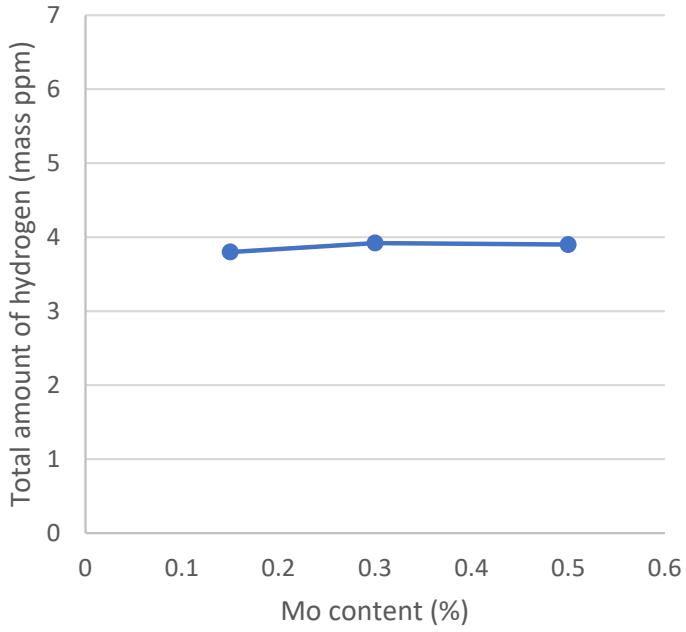


Figure 18. Influence of the Mo content on the total amount of stored hydrogen in samples immersed in a 10% ammonium thiocyanate solution for 48 h after BH treatment.

Figure 19 shows the result of 3DAP analysis of 0.5% Mo-added steel (Mo4). Mo is segregated at the grain boundary and Mo-containing precipitates were not observed. This observation suggests that the main cause for the positive effect of Mo on delayed fracture resistance is the increase in grain boundary cohesion due to the segregation of Mo. To confirm this hypothesis, an experiment was carried out by varying the degree of the grain boundary segregation.

Figure 20 shows the effect of the heating pattern on the time to the delayed fracture of steels Mo1–Mo4. The samples designated as "long" were heated at 10 °C/s to 900 °C and held for 300 s, whereas the samples designated as "short" were heated at 10 °C/s to 875 °C, quenched immediately after heating, and subjected to BH treatment. The segregation of Mo is facilitated during the prolonged annealing. It is clearly observed that the longer heating time significantly increased the time to the delayed fracture, even though the prior austenite grain size of the "long" samples was larger than that of the "short" samples. These observations provide clear evidence that the major cause of the increase in time to the delayed fracture with the Mo addition correlates with the intensity of the Mo segregation. This can be due to an increase in grain boundary cohesion by the presence of Mo atoms counteracting the deleterious HEGBDE effect. This beneficial effect of Mo on the grain boundary cohesion has been derived by ab initio calculations [49] as well as by thermodynamic considerations [50]. In addition, Ito et al. [51] reported, based on first-principles calculations, that the Mo segregation suppresses the H segregation due to the repulsive interaction between Mo and H atoms. The reduction of the H segregation

consequently increases the grain boundary cohesion and the time to a delayed fracture. The strong beneficial effect of the Mo addition on delayed fracture resistance is attributed to the synergistic effect of increasing Mo intergranular segregation and reducing H segregation.

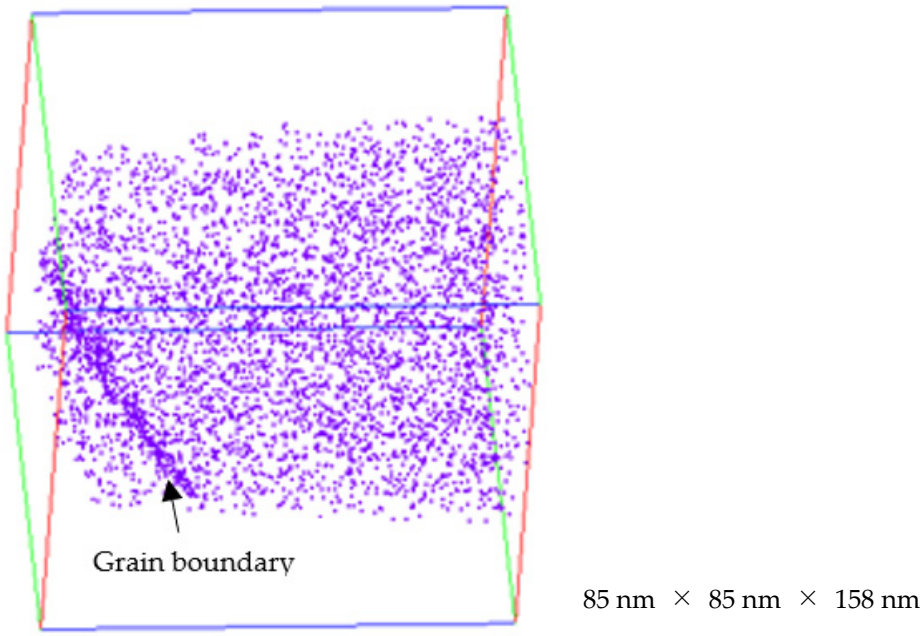


Figure 19. Distribution of Mo in steel Mo 4 containing 0.5% Mo measured using 3D-AP.

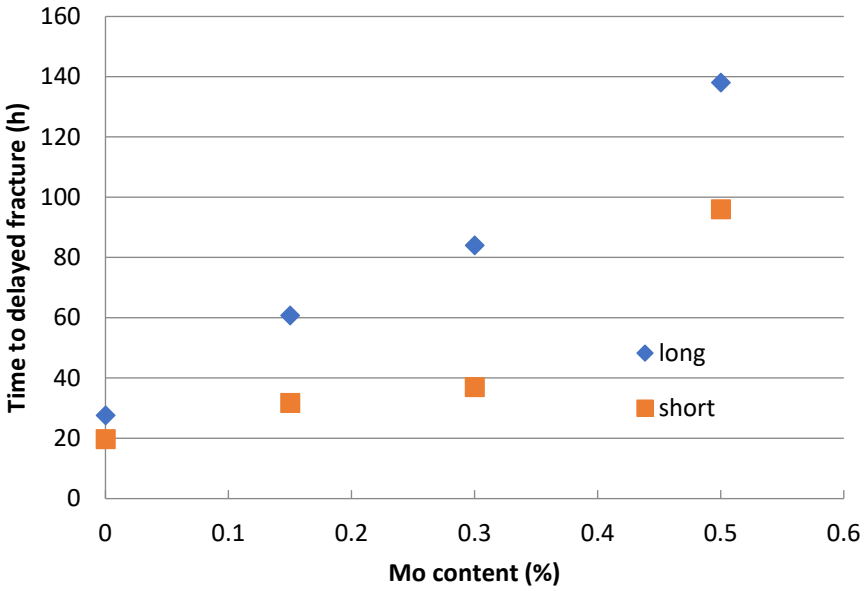


Figure 20. Effect of Mo content and heating patterns on time to delayed fracture. Long: 900 °C × 300 s; short: 875 °C without holding.

In addition to Nb and Mo, the effect of B on the susceptibility to a delayed fracture was investigated because the reported results were quite conflicting. Nie et al. [52] reported that the resistance to the delayed fracture increased with the increasing B addition. Li et al. [53] reported that the effect of the B addition on the susceptibility to the delayed fracture was weak if the hydrogen charging was mild; however, in the case of severe charging, the susceptibility to the delayed fracture decreased with an increasing amount of B. The insignificant effect of B was also reported by Komazaki et al. [54].

In order to investigate the conflicting statements, the effect of B on the susceptibility to a delayed fracture of hot-stamped ultrahigh-strength steels was investigated using the steels B0 without B and Nb3 with 0.002% B in Table 1. The respective samples were heated to 825 °C at 10 °C/s and then quenched and BH treated. The delayed fracture test results demonstrated that the time to the delayed fracture of Steel B0 was 13.9 h and that of Nb3 was 15.8 h, as shown in Figure 21, respectively. Thus, the significant effect of the B addition regarding the delayed cracking resistance is not obvious. However, it is well established that the addition of a few mass ppm of B significantly improves the resistance to the secondary cracking of interstitial-free (IF) steels and pure irons [55]. An ab initio calculation of the increase in the grain boundary cohesion due to the B addition supports this result [56,57].

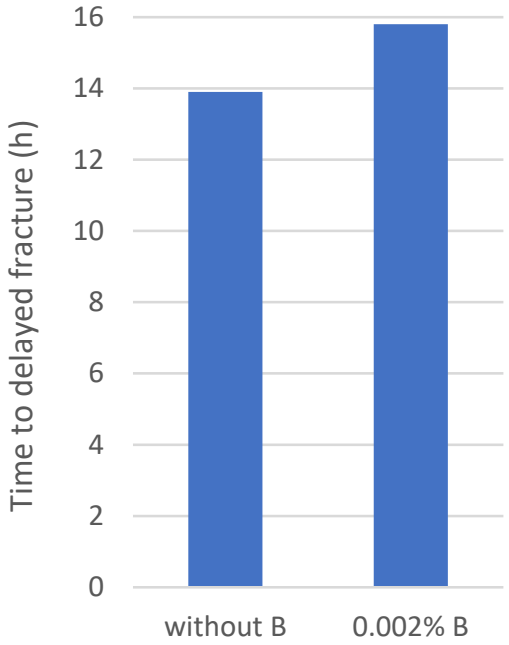


Figure 21. Effect of B on time to delayed fracture of steels B0 and Nb3.

The difference between IF steels and ultrahigh-strength steels is that in the latter, carbon co-segregates with boron. The amounts of C and B segregated at the grain boundary can be calculated thermodynamically according to Hillert's assumption that the grain boundary is treated as a phase and the parallel tangent law is applied between the Gibbs free energy of this phase and that of the matrix phase. The calculation assumes that the thermodynamic data for the grain boundary phase are identical to those for the liquid phase. The thermodynamic calculation demonstrated that the segregation of B suppressed the segregation of C. Since C also increases the grain boundary cohesion [56,58], this may be the reason why the B addition did not demonstrate a clear improvement in the resistance to the delayed fracture of high-strength steels.

Finally, an example of an improved delayed fracture resistance through proper alloy design is provided. Figure 22 demonstrates the time to the delayed fracture of Nb- and Mo-containing hot-stamped 2000 MPa class steel sheet (Steel NM) and that of 1500 MPa-class commercial steel (Steel A). This result underlines that the resistance to the delayed fracture of a 2000 MPa-class steel can be improved to a level higher than that of a commercial 1500 MPa-class steel through appropriate alloy design. This improvement in the delayed fracture resistance is presumed mainly due to grain refinement and an increase in grain boundary cohesion by the addition of Nb and Mo.

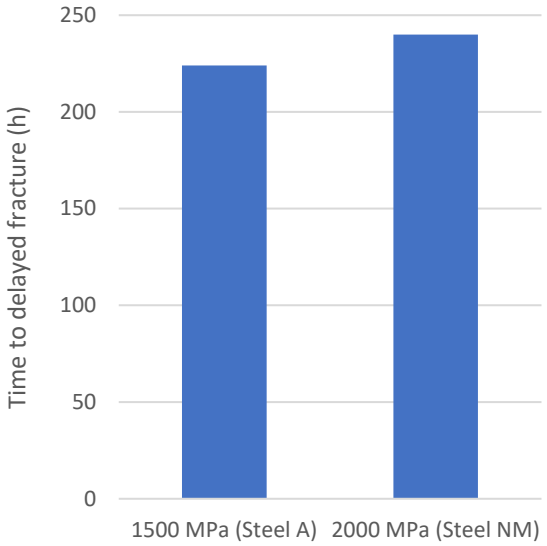


Figure 22. Time to delayed fracture of properly alloy-designed 2000 MPa-class steel versus commercial 1500 MPa-class steel.

4. Concluding Remarks

This paper investigated the influence of microstructural control and the alloy design on improving the resistance to the delayed fracture of ultra-high strength automotive sheet steels in general, and for hot-stamped steels in particular.

Proper microstructural control such as grain refinement, appropriate introduction of ferrite and retained austenite as a second phase, and surface decarburization were demonstrated to increase the resistance to a delayed fracture, respectively.

Regarding alloy design, the effects of Nb, Mo, and B on the resistance to the delayed fracture of 2000 MPa-class hot-stamped and BH-treated steel sheets were investigated in detail. The results demonstrated a significant increase in the resistance to the delayed fracture by adding Nb and Mo, and the underlying mechanisms were discussed.

It was clarified that the improvement of delayed fracture resistance is mainly due to the increase in grain boundary cohesion by the intergranular segregation of microalloys and grain refinement. Since the alloy carbides are covered by iron carbides and BH treatment in hot-stamped steels, their ability as hydrogen trapping sites is reduced. In particular, molybdenum alloy provided clear evidence that the effect of grain boundary segregation plays the main role in improving the resistance to the delayed fracture. The delayed fracture time of the 0.5% added steel increased nearly seven times longer than that of the Mo-free steel by heat treatment at 900 °C for 5 min, which promotes the grain boundary segregation.

By applying a proper microstructural control and alloy design, it was demonstrated that the delayed fracture resistance of 2000 MPa-class hot stamped steel can be increased to above that of conventional 1500 MPa press-hardening steel.

Author Contributions: Conceptualization, T.S., H.M. and M.O.; methodology, T.S. and H.M.; experimental investigation, T.S. and M.O.; writing—original draft preparation, T.S.; review and final editing, M.O., H.M. and T.S.; funding acquisition, H.M. All authors have read and agreed to the published version of the manuscript.

Funding: This research was funded by the Companhia Brasileira de Metalurgia e Mineracao (CBMM), Sao Paulo, Brazil and the International Molybdenum Association (IMOA), London, UK.

Data Availability Statement: No applicable.

Acknowledgments: The authors wish to sincerely thank J. Takahashi, Nippon Steel, for providing the analytical results of atom probe tomography data and fruitful discussion, and Tatsuya Tokunaga, Kyushu Institute of Technology, for thermodynamically calculating the grain boundary segregation of alloys.

Conflicts of Interest: The authors declare no conflict of interest.

References

1. JFE Steel. Available online: https://www.jfe-steel.co.jp/release/2020/12/201223.html (accessed on 11 June 2023).
2. Arcelor Mittel. Available online: https://automotive.arcelormittal.com/products/flat/PHS/usibor_ductibor (accessed on 11 June 2023).
3. Nakazawa, Y.; Yoshida, T.; Niwa, T.; Kawachi, T.; Nakata, M.; Uenishi, A.; Hiwatashi, S. Development of Future Automobile Design Concept, NSafe™-AutoConcept. *Nippon Steel Tech. Rep.* **2019**, *412*, 2–6. Available online: https://www.nipponsteel.com/en/tech/report/pdf/122-02.pdf (accessed on 11 June 2023).
4. Oriani, R.A.; Josephic, P.H. Equilibrium aspects of hydrogen-induced cracking of steels. *Acta Metall.* **1974**, *22*, 1065–1074. [CrossRef]
5. Gerberich, W.W.; Oriani, R.A.; Lji, M.J.; Chen, X.; Foecke, T. The necessity of both plasticity and brittleness in the fracture thresholds of iron. *Philos. Mag. A* **1991**, *63*, 363–376. [CrossRef]
6. Birnbaum, H.K.; Sofronis, P. Hydrogen-enhanced localized plasticity—A mechanism for hydrogen-related fracture. *Mater. Sci. Eng. A* **1994**, *176*, 191–202. [CrossRef]
7. Sofronis, P.; Birnbaum, H.K. Mechanics of the hydrogen-dislocation-inpurity interactions. *J. Mech. Phys. Solids* **1995**, *43*, 49–90. [CrossRef]
8. Nagao, A.; Dadfarnia, M.; Somerday, B.P.; Sofronis, P.; Ritchie, R.O. Hydrogen-enhanced-plasticity mediated decohesion for hydrogen-induced intergranular and "quasi-cleavage" fracture of lath martensitic steels. *J. Mech. Phys. Solids* **2018**, *112*, 403–430. Available online: https://www2.lbl.gov/ritchie/Library/PDF/2018_Nagao_H_Enchanced_Plasticity.pdf (accessed on 11 June 2023). [CrossRef]
9. Lynch, S.P. Environmentally assisted cracking: Overview of evidence for an adsorption-induced localized-slip process. *Acta Metall.* **1988**, *36*, 2639–2661. [CrossRef]
10. Nagumo, M. Hydrogen related failure of steels—A new aspect. *Mater. Sci. Technol.* **2004**, *8*, 940–950. [CrossRef]
11. Robertson, I.M.; Sofronis, P.; Nagao, A.; Martin, M.L.; Wang, S.; Gross, D.W.; Nygren, K.E. Hydrogen Embrittlement Understood. *Metall. Mater. Trans. A* **2015**, *46A*, 2323–2341. Available online: https://link.springer.com/article/10.1007/s11661-015-2836-1 (accessed on 11 June 2023). [CrossRef]
12. Fuchigami, H.; Minami, H.; Nagumo, M. Effect of grain size on the susceptibility of martensitic steel to hydrogen-related failure. *Philos. Mag. Lett.* **2006**, *86*, 21–29. [CrossRef]
13. Takazawa, K.; Wada, Y.; Ishigaki, R.; Kayano, R. Effects of Grain Size on Hydrogen Environment Embrittlement of High Strength Low Alloy Steel in 45 MPa Gaseous Hydrogen. *J. Jpn. Inst. Met.* **2010**, *74*, 520–526. [CrossRef]
14. Cho, L.; Bradley, P.E.; Lauria, D.S.; Connolly, M.J.; Seo, E.J.; Findley, K.O.; Speer, J.G.; Golem, L.; Slifka, A.J. Effects of hydrogen pressure and prior austenite grain size on the hydrogen embrittlement characteristics of a press-hardened martensitic steel. *Int. J. Hydrogen Energy* **2021**, *46*, 24425–24439. [CrossRef]
15. Speer, J.; Matlock, D.K.; De Cooman, B.C.; Schroth, J.G. Carbon partitioning into austenite after martensite transformation. *Acta Mater.* **2003**, *51*, 2611. [CrossRef]
16. Seo, E.J.; Cho, L.; Charles, B.; De Cooman, B.C. Application of Quenching and Partitioning (Q&P) Processing to Press Hardening Steel. *Metall. Mater. Trans. A* **2014**, *45A*, 4022–4037.
17. Han, X.H.; Zhong, Y.Y.; Tan, S.L.; Ding, Y.N.; Chen, J. Microstructure and performance evaluations on Q&P hot stamping parts of several UHSS sheet metals. *Sci. China Technol. Sci.* **2017**, *60*, 1692–1701.
18. Han, X.; Zhong, Y.; Xin, P. Research on one-step quenching and partitioning treatment and its application in hot stamping process. *Proc. Inst. Mech. Eng. Part B J Eng. Manuf.* **2015**, *84*, 163–182. [CrossRef]
19. Nishimura, R.; Tanaka, Y.; Miyagi, T.; Ogawa, M.; Otsuka, K.; Nakazawa, Y. Development of Forming Methods for Functional Improvement of Car Body Structural Parts. *Nippon. Steel Tech. Rep.* **2019**, *122*, 13–19. Available online: https://www.nipponsteel.com/en/tech/report/pdf/122-04.pdf (accessed on 11 June 2023).
20. Bian, J.; Mohrbacher, H.; Zhan, S.; Lu, H.; Wang, W.; Zhang, Y.; Wang, L. Impact of Nb Microalloying on the Hydrogen Embrittlement of Press Hardening Steel. In Proceedings of the 5th International Conference Hot Sheet Metal Forming of High Performance Steel, Toronto, ON, Canada, 31 May–3 June 2015; pp. 65–74.
21. Zhang, S.; Huang, Y.; Sun, B.; Liao, Q.; Lu, H.; Jian, B.; Mohrbacher, H.; Zhang, W.; Guo, A.; Zhang, Y. Effect of Nb on hydrogen-induced delayed fracture in high strength hot stamping steels. *Mater. Sci. Eng. A* **2015**, *626*, 136–143. [CrossRef]
22. Okayasu, M.; Sato, M.; Ishida, D.; Senuma, T. The effect of precipitations (NbC and carbide) in Fe-C-MnxNb steels on hydrogen embrittlement characteristics. *Mater. Sci. Eng. A* **2020**, *791*, 139598. [CrossRef]
23. Zhang, C.; Hui, W.; Zhao, X.; Zhang, Y.; Zhao, X. The potential significance of microalloying with Nb in enhancing the resistance to hydrogen-induced delayed fracture of 1300-MPa-grade high-strength bolt steel. *Eng. Fail. Anal.* **2022**, *135*, 106144. [CrossRef]
24. Taniguchi, S.; Kameya, M.; Kobayashi, Y.; Ito, K.; Yamasaki, S. Hydrogen Trapping and Precipitation of Alloy Carbides in Molybdenum Added Steels and Vanadium Added Steels. *Tetsu-to-Hagané* **2023**, *109*, 438–449. [CrossRef]
25. Kimura, Y.; Moronaga, T.; Inoue, T. Influence of Thermomechanical Treatment on Delayed Fracture Property of Mo-Bearing Medium-Carbon Steel. *ISIJ Int.* **2022**, *62*, 377–388. [CrossRef]

26. Yoo, J.; Jo, M.C.; Kim, S.; Kim, S.-H.; Oh, J.; Sohn, S.S.; Lee, S. Effects of solid solution and grain-boundary segregation of Mo on hydrogen embrittlement in 32MnB5 hot-stamping steels. *Acta Mater.* **2021**, *207*, 116661. [CrossRef]
27. Jo, M.C.; Yoo, J.; Kim, S.; Kim, S.; Oh, J.; Bian, J.; Sohn, S.S.; Lee, S. Effects of Nb and Mo alloying on resistance to hydrogen embrittlement in 1.9 GPa-grade hot-stamping steels. *Mater. Sci. Eng. A* **2020**, *789*, 139656. [CrossRef]
28. Yamazaki, S.; Kubota, M.; Tarui, T. Evaluation Method for Delayed Fracture Susceptibility of Steels and Development of High Tensile Strength Steels with High Delayed Fracture Resistance. *Nippon. Steel Tech. Rep.* **1999**, *80*, 50–55. Available online: https://www.nipponsteel.com/en/tech/report/nsc/pdf/8011.pdf (accessed on 11 June 2023).
29. Cho, L.; Seo, E.J.; Sulistiyo, D.H.; Jo, K.R.; Kim, S.W.; Oh, J.K.; Cho, Y.R.; De Cooman, B.C. Influence of vanadium on the hydrogen embrittlement of aluminized ultra-high strength press hardening steel. *Mater. Sci. Eng. A* **2018**, *735*, 448–455. [CrossRef]
30. Chen, W.-J.; Gao, P.-F.; Wang, S.; Lu, H.-Z.; Zhao, Z.-Z. Effect of vanadium on hydrogen embrittlement susceptibility of high-strength hot-stamped steel. *J. Iron Steel Res. Int.* **2021**, *28*, 211–222.
31. Wei, F.G.; Tsuzaki, K. Quantitative analysis on hydrogen trapping of TiC particles in steel. *Metall. Mater. Trans. A* **2006**, *37*, 331–353. [CrossRef]
32. Wei, F.G.; Hara, T.; Tsuzaki, K. High-resolution transmission electron microscopy study of crystallography and morphology of TiC precipitates in tempered steel. *Philos. Mag.* **2004**, *84*, 1735–1751. [CrossRef]
33. Tokizawa, T.; Yamamoto, K.; Takemoto, Y.; Senuma, T. Development of 2000 MPa Class Hot Stamped Steel Components with Good Toughness and High Resistance against Delayed Fracture. In Proceedings of the 4th International Conference Hot Sheet Metal Forming of High Performance Steel, Lulea, Sweden, 9–12 June 2013; pp. 473–479.
34. Mohrbacher, H. Property Optimization in As-Quenched Martensitic Steel by Molybdenum and Niobium Alloying. *Metals* **2018**, *8*, 234. [CrossRef]
35. Pan, H.; Li, X.; Qiao, B.; Zhang, Y.; Miao, N.; Liu, L.; Ding, H.; Cai, M. New Insights to Understand the Influence of Nb/Mo on Hydrogen Embrittlement Resistance of Warm-Rolled Medium-Mn Steels. *J. Mater. Eng. Perform.* **2022**, *31*, 3228–3233. [CrossRef]
36. Mohrbacher, H.; Senuma, T. Alloy Optimization for Reducing Delayed Fracture Sensitivity of 2000 MPa Press Hardening Steel. *Metals* **2020**, *10*, 853. [CrossRef]
37. Zhang, S.; Qi, L.; Liu, S.; Peng, Z.; Cheng, Y.F.; Huang, F.; Liu, J. Synergistic effects of Nb and Mo on hydrogen-induced cracking of pipeline steels: A combined experimental and numerical study. *J. Mater. Sci. Technol.* **2023**, *158*, 156–170. [CrossRef]
38. Yoo, J.; Jo, M.C.; Bian, J.; Sohn, S.S.; Lee, S. Effects of Nb or (Nb + Mo) alloying on Charpy impact, bending, and delayed fracture properties in 1.9-GPa-grade press hardening steels. *Mater. Charact.* **2021**, *176*, 111133. [CrossRef]
39. Tateyama, S.; Ishio, R.; Hayashi, K.; Sue, T.; Takemoto, Y.; Senuma, T. Microstructures and Mechanical Properties of V and/or Nb Bearing Ultrahigh Strength Hot Stamped Steel Components. *Tetsu-to-Hagané* **2014**, *100*, 1114–1122. [CrossRef]
40. Zhang, C.; Hui, W.; Zhao, X.; Zhang, Y.; Zhao, X. Hydrogen-induced delayed fracture behaviour of V + Nb-microalloyed high-strength bolt steel with internal and environmental hydrogen. *Corros. Sci.* **2022**, *209*, 110710. [CrossRef]
41. Gui, L.; Zhao, Y.; Feng, Y.; Ma, M.; Lu, H.; Tan, K.; Chiu, P.-H.; Guo, A.; Bian, J.; Yang, J.-R.; et al. Study on the improving effect of Nb-V microalloying on the hydrogen induced delayed fracture property of 22MnB5 press hardened steel. *Mater. Des.* **2023**, *227*, 111763. [CrossRef]
42. Zhang, S.; Liu, S.; Wan, J.; Liu, W. Effect of Nb–Ti multi-microalloying on the hydrogen trapping efficiency and hydrogen embrittlement susceptibility of hot-stamped boron steel. *Mater. Sci. Eng. A* **2020**, *772*, 138788. [CrossRef]
43. Yoo, J.; Jo, M.C.; Kim, S.; Oh, J.; Bian, J.; Sohn, S.S.; Lee, S. Effects of Ti alloying on resistance to hydrogen embrittlement in (Nb + Mo)-alloyed ultra-high-strength hot-stamping steels. *Mater. Sci. Eng. A* **2020**, *22*, 139763. [CrossRef]
44. Miyamoto, G.; Iwata, N.; Takayama, N.; Furuhara, T. Mapping the parent austenite orientation reconstructed from the orientation of martensite by EBSD and its application to ausformed martensite. *Acta Mater.* **2010**, *58*, 6393–6403. [CrossRef]
45. Yamamoto, K.; Hidaka, K.; Morioka, K.; Sue, T.; Takemoto, Y.; Senuma, T. Microstractural Control for Improving Productivity and Mechanical Properties of Hot-Stamped Products. *Jpn. Soc. Technol. Plast.* **2013**, *54*, 137–142. [CrossRef]
46. Watanabe, J.; Takai, K.; Nagumo, M. Improvement of Delayed Fracture Strength of High Strength Steels by Intergranular Ferrite Precipitation. *Tetsu-to-Hagané* **1996**, *82*, 947–952. [CrossRef] [PubMed]
47. Kim, J.S.; Lee, Y.H.; Lee, D.L.; Park, K.-T.; Lee, C.S. Effect of Intergranular Ferrite on Hydrogen Delayed Fracture Resistance of Ultrahigh Strength Boron-added Steel. *ISIJ Int.* **2007**, *47*, 913–919. [CrossRef]
48. Tokunaga, T.; Motomura, Y.; Era, H.; Tsuchiyama, T.; Shobu, K.; Hasebe, M.; Ohtani, H. Effect of Alloying Elements on Grain Boundary Segregation of Boron and Carbon in α-Iron. *Tetsu-to-Hagané* **2023**, *109*, 158–166. [CrossRef]
49. Geng, W.-T.; Freeman, A.J.; Olson, G.B. Influence of alloying additions on grain boundary cohesion of transition metals: First-principles determination and its phenomenological extension. *Phys. Rev. B* **2001**, *63*, 165415. [CrossRef]
50. Lejcek, P. *Grain Boundary Segregation in Metals*; Springer Series in Materials Science: Berlin/Heidelberg, Germany, 2010; pp. 173–183.
51. Ito, K.; Tanaka, Y.; Tsutsui, K.; Omura, T. Effect of Mo addition on hydrogen segregation at α-Fe grain boundaries: A first-principles investigation of the mechanism by which Mo addition improves hydrogen embrittlement resistance in high-strength steels. *Comput. Mater. Sci.* **2023**, *218*, 111951. [CrossRef]
52. Nie, Y.; Hui, W.; Fu, W.; Weng, Y. Effect of Boron on Delayed Fracture Resistance of Medium-Carbon High Strength Spring Steel. *J. Iron Steel Res. Int.* **2007**, *14*, 53–57. Available online: https://link.springer.com/article/10.1016/S1006-706X%2807%2960090-9 (accessed on 11 June 2023). [CrossRef]

53. Li, H.; Cheng, X.Y.; Shen, H.P.; Su, L.C.; Zhang, S.Y. Effect of Boron Microalloying Element on Susceptibility to Hydrogen Embrittlement in High Strength Mooring Chain Steel. In *HSLA Steels 2015, Microalloying 2015 & Offshore Engineering Steels*; Springer: Berlin/Heidelberg, Germany, 2015; pp. 1211–1218. Available online: https://link.springer.com/chapter/10.1007/978-3-319-48767-0_151 (accessed on 11 June 2023).
54. Komazaki, S.; Watanabe, S.; Misawa, T. Influence of Phosphorus and Boron on Hydrogen Embrittlement Susceptibility of High Strength Low Alloy Steel. *ISIJ Int.* **2003**, *43*, 1851–1857. [CrossRef]
55. Fudanoki, F.; Sumitomo, H. Effect of Grain Size and Boron on Resistance to Secondary Working Embrittlement of High-purity Ferritic Stainless Cold-rolled Steel Sheet. *Tetsu-to-Hagané* **1998**, *84*, 804–810. Available online: https://www.jstage.jst.go.jp/article/tetsutohagane1955/84/11/84_11_804/_pdf (accessed on 11 June 2023). [CrossRef]
56. Yamaguchi, M. First-Principles Calculations of the Grain-Boundary Cohesive Energy. *J. Jpn. Inst. Met.* **2008**, *72*, 657–666. [CrossRef]
57. Kulkov, S.S.; Bakulin, A.V.; Kulkova, S.E. Effect of boron on the hydrogen-induced grain boundary embrittlement in α-Fe. *Int. J. Hydrog. Energy* **2023**, *43*, 1909–1925. [CrossRef]
58. Kimura, A.; Kimura, H. Effect of Carbon on the Hydrogen Induced Grain Boundary Fracture in Iron. *J. Jpn. Inst. Met.* **1983**, *47*, 807–813. Available online: https://www.jstage.jst.go.jp/article/jinstmet1952/47/10/47_10_807/_pdf (accessed on 11 June 2023). [CrossRef]

Disclaimer/Publisher's Note: The statements, opinions and data contained in all publications are solely those of the individual author(s) and contributor(s) and not of MDPI and/or the editor(s). MDPI and/or the editor(s) disclaim responsibility for any injury to people or property resulting from any ideas, methods, instructions or products referred to in the content.